

Two-Photon Dynamics in Coherent Rydberg Atomic Ensemble

Bing He,^{1,2} A. V. Sharypov,^{3,4} Jiteng Sheng,² Christoph Simon,¹ and Min Xiao^{2,5,*}

¹*Institute for Quantum Science and Technology, University of Calgary, Calgary, Alberta T2 N 1N4, Canada*

²*Department of Physics, University of Arkansas, Fayetteville, Arkansas 72701, USA*

³*Kirensky Institute of Physics, 50 Akademgorodok, Krasnoyarsk 660036, Russia*

⁴*Siberian Federal University, 79 Svobodny Avenue, Krasnoyarsk 660041, Russia*

⁵*National Laboratory of Solid State Microstructures and School of Physics, Nanjing University, Nanjing 210093, China*

(Received 19 December 2013; published 4 April 2014)

We study the interaction of two photons in a Rydberg atomic ensemble under the condition of electromagnetically induced transparency, combining a semiclassical approach for pulse propagation and a complete quantum treatment for quantum state evolution. We find that the blockade regime is not suitable for implementing photon-photon cross-phase modulation due to pulse absorption and dispersion. However, approximately ideal cross-phase modulation can be realized based on relatively weak interactions, with counterpropagating and transversely separated pulses.

DOI: 10.1103/PhysRevLett.112.133606

PACS numbers: 42.50.Nn, 32.80.Ee, 34.20.Cf, 42.50.Gy

Strong nonlinearity at the single-photon level is desirable for the realization of all-optical quantum devices. Ensembles of highly excited Rydberg atoms under the electromagnetically induced transparency (EIT) condition combine the advantages of strong atom-field coupling without significant absorption and nonlocal atomic interaction and have attracted intensive experimental [1–7] and theoretical studies [8–17] recently. The strong correlation directly between single photons inside the Rydberg atomic ensemble was observed [7], and the formation of a Wigner crystal of individual photons is also predicted [15]. When such interaction is applied to implement the cross-phase modulation (XPM) between two individual photons with a nonzero relative velocity as in Fig. 1 [18–21], a main difference from a single probe beam propagation in Rydberg EIT medium [1–17] is that no steady state exists for the pulses, because their interaction varies with the relative distance, pulse velocity that changes pulse sizes, as well as the absorption in the medium. The realistic time dependence in the inherent nonlinear dynamics makes a complete solution of the problem rather challenging. With the combination of a semiclassical approach for pulse propagation and a complete quantum approach for pulse quantum state evolution, we find a realistic picture for the dynamical process by showing the concerned figures of merit. We show that our proposed setup outperforms the previously considered Rydberg blockade regime [20] clearly in terms of much lower photon absorption and negligible group velocity dispersion.

The detailed two-photon XPM via Rydberg EIT is as follows. One respectively couples the far-away input photons to cold Rydberg atoms under the EIT condition to form the light-matter quasiparticle called the dark-state polariton (DSP) [22]. The spatial distribution of the pulses necessitates a quantum many-body description of the

process. The prepared DSPs are in the state $|1\rangle_l = \int d^3x f_l(\mathbf{x}) \hat{\Psi}_l^\dagger(\mathbf{x}) |0\rangle$ for $l = 1, 2$, where $f_l(\mathbf{x})$ are their snapshots with $\int d^3x |f_l(\mathbf{x})|^2 = 1$ and with $\hat{\Psi}(\mathbf{x}) = \cos\theta \hat{\mathcal{E}}(\mathbf{x}) - \sin\theta \hat{\mathcal{S}}(\mathbf{x})$ as the superposition of electromagnetic field operator $\hat{\mathcal{E}}(\mathbf{x})$, where Rydberg spin-wave field operator $\hat{\mathcal{S}}(\mathbf{x})$ is the DSP field operator. The many-body version of the atom-field Hamiltonian

$$\begin{aligned} H_{\text{AF}}^l &= -\frac{1}{2} \int d^3x \{ \Omega_c \hat{\mathcal{S}}_l^\dagger(\mathbf{x}) \hat{P}_l(\mathbf{x}) + g \sqrt{N} \hat{\mathcal{E}}_l^\dagger(\mathbf{x}) \hat{P}_l(\mathbf{x}) + \text{H.c.} \} \\ &\quad + \int d^3x \Delta_l \hat{P}_l^\dagger(\mathbf{x}) \hat{P}_l(\mathbf{x}) \\ &= - \int d^3x \{ \omega^+ \hat{\Phi}_{+,l}^\dagger \hat{\Phi}_{+,l}(\mathbf{x}) + \omega^- \hat{\Phi}_{-,l}^\dagger \hat{\Phi}_{-,l}(\mathbf{x}) \} \end{aligned} \quad (1)$$

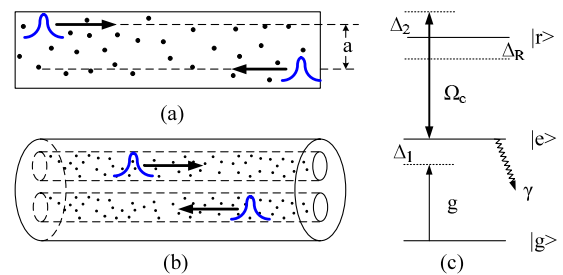


FIG. 1 (color online). (a) Two single-photon pulses propagate in a Rydberg atomic ensemble. (b) Two pulses propagate in two parallel waveguides filled with Rydberg atoms. For the insignificant diffraction or the propagation in (b), the pulse profiles for the numerical simulations in Figs. 3 and 4 can be approximated as one dimensional. (c) Atomic level scheme for the system. Without pulse interaction there is $\Delta_1 + \Delta_2 = 0$ under the EIT condition. Here, $\Delta_1 = \omega_{eg} - \omega_p$ and $\Delta_2 = \omega_{re} - \omega_c$ (ω_p is the input pulses' central frequency, and ω_c is the frequency of the pump beam). The Rydberg level is shifted by Δ_R due to the interaction with another pulse.

($\hbar = 1$) also involving the polarization field $\hat{P}(\mathbf{x})$ for the excited level $|e\rangle$ can be diagonalized in terms of two bright-state polariton (BSP) fields $\hat{\Phi}_+(\mathbf{x}) = \sin\theta \sin\phi \hat{\mathcal{E}}(\mathbf{x}) + \cos\phi \hat{P}(\mathbf{x}) + \cos\theta \sin\phi \hat{S}(\mathbf{x})$ and $\hat{\Phi}_-(\mathbf{x}) = \sin\theta \cos\phi \hat{\mathcal{E}}(\mathbf{x}) - \sin\phi \hat{P}(\mathbf{x}) + \cos\theta \cos\phi \hat{S}(\mathbf{x})$, where their spectrum $\omega^\pm = \frac{1}{2}(\Delta_1 \pm \sqrt{\Delta_1^2 + g^2 N + \Omega_c^2})$ is a function of the input photon detuning Δ_1 , pump beam Rabi frequency Ω_c , and atom density N . The combination coefficients for the polariton field operators satisfy the relations $\tan\theta = g\sqrt{N}/\Omega_c$ and $\tan 2\phi = \sqrt{g^2 N + \Omega_c^2}/\Delta_1$ with g as the atom-field coupling constant. When the DSPs get close to each other, the interaction

$$H_I = \int d^3x d^3x' \hat{S}_1^\dagger(\mathbf{x}) \hat{S}_2^\dagger(\mathbf{x}') \Delta(\mathbf{x} - \mathbf{x}') \hat{S}_2(\mathbf{x}') \hat{S}_1(\mathbf{x}) \quad (2)$$

between the pulses takes effect. Here, we consider the van der Waals (VdW) potential $\Delta(\mathbf{x}) = -C_6/|\mathbf{x}|^6$ in the Rydberg atomic ensemble. Such interaction, however, also causes the transition of DSP to BSPs containing $\hat{P}_l(\mathbf{x})$ components decaying at the rate γ . The decay of the $\hat{P}_l(\mathbf{x})$ field is described by [23]

$$H_D^l = i\sqrt{\gamma} \int d^3x \{ \hat{P}_l(\mathbf{x}) \hat{\xi}_l^\dagger(\mathbf{x}, t) - \hat{P}_l^\dagger(\mathbf{x}) \hat{\xi}_l(\mathbf{x}, t) \}, \quad (3)$$

with the white-noise operators of the reservoirs satisfying $[\hat{\xi}_l(\mathbf{x}, t), \hat{\xi}_l^\dagger(\mathbf{x}', t')] = \delta^3(\mathbf{x} - \mathbf{x}') \delta(t - t')$. The evolved pulse quantum state under all above mentioned factors should be close to the ideal output $e^{i\varphi} |1\rangle_1 |1\rangle_2$ (φ is a uniform one) for realizing a photon-photon XPM.

Before studying the input's quantum state evolution, one needs to ascertain the pulses' propagation in the medium so that their interaction time should be known. The absorption and dispersion of the pulses can be found in a semiclassical approach [24,25] that treats the input pulses as the classical fields $E_l(\mathbf{x})$, which are equivalent to the averages $\langle \hat{\mathcal{E}}_l(\mathbf{x}) \rangle$ of the quantum fields (up to a constant). In this framework, the atom-field coupling is described by the following equations for the atomic density matrix elements [24]:

$$\dot{\rho}_{eg} = -\left(\frac{\gamma_{eg}}{2} + i\Delta_1\right) \rho_{eg} + i\frac{\mu_{eg}}{2} E_l (\rho_{ee} - \rho_{gg}) - i\frac{\Omega_c}{2} \rho_{rg}, \quad (4a)$$

$$\dot{\rho}_{rg} = -\left(\frac{\gamma_{rg}}{2} + i(\Delta_1 + \Delta_2 + \Delta_R)\right) \rho_{rg} - i\frac{\Omega_c}{2} \rho_{eg} + i\frac{\mu_{eg}}{2} E_l \rho_{re}, \quad (4b)$$

where μ_{ij} are the transition dipole matrix elements and γ_{ij} are the decay rates of the relevant levels. The interaction with another pulse shifts the energy level of $|r\rangle$ and, hence, adds an extra term $\Delta_R(\mathbf{x}, t) = \sin^2\theta T(t) \int d^3x' \Delta(\mathbf{x} - \mathbf{x}') \langle \hat{\Psi}_{3-l}^\dagger \hat{\Psi}_{3-l} \rangle(\mathbf{x}', t)$ to the detuning Δ_2 of the pump beam,

where $T(t)$ is the time-dependent transmission rate. This practice of reducing the interaction effect to a c -number detuning Δ_R is equivalent to a mean field treatment for the spin-wave fields in Eq. (2). One has the time-dependent solution

$$\begin{pmatrix} \rho_{eg}(t) \\ \rho_{rg}(t) \end{pmatrix} = -i\frac{1}{2}\mu_{eg} \int_0^t d\tau e^{\int_\tau^t dt' \hat{M}(t')} \begin{pmatrix} E_l \\ 0 \end{pmatrix} \quad (5)$$

to Eqs. (4a) and (4b) under the weak drive approximation [24,25] for single photons, where

$$\hat{M}(t) = \begin{pmatrix} -\left(\frac{\gamma}{2} + i\Delta_1\right) & -i\frac{\Omega_c}{2} \\ -i\frac{\Omega_c}{2} & -\frac{\gamma_{rg}}{2} - i(\Delta_1 + \Delta_2 + \Delta_R(t)) \end{pmatrix}$$

with $\gamma_{eg} = \gamma$. It is straightforward to obtain the time-dependent refractive index and decay rate from the susceptibility $\chi^{(1)}(t) = -2N\mu_{eg}\rho_{eg}(t)/(\epsilon_0 E_l)$ based on Eq. (5).

When two pulses approach each other, one phenomenon that could happen is known as the Rydberg blockade. For the red-detuned photons ($\Delta_1 > 0$) the rising magnitude of negative Δ_R constantly shifts the refractive index curve going through the EIT point at a certain detuning Δ_1 toward that of the corresponding two-level system. In the limit $|\Delta_R| \gg \gamma$, the system will virtually turn into a two-level one; see Fig. 2(a). One signature of the Rydberg blockade is a platform of nearly unchanging group velocity shown in Fig. 2(b). In the blockade regime, the pulse group velocity asymptotically tends to that of the corresponding two-level system; only those with $\Delta_1 \leq 0.5\gamma$ in Fig. 2 can reach the speed of light c with growing negative Δ_R .

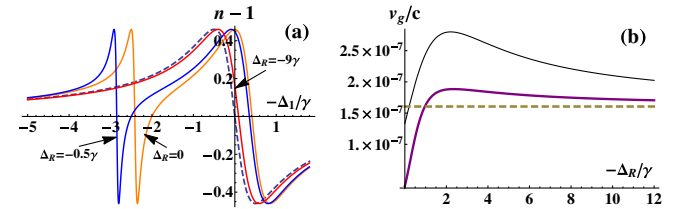


FIG. 2 (color online). (a) Shift of refractive curves with increasing $\Delta_R < 0$. Here, $n - 1 = 1/2 \text{Re}\{\chi^{(1)}\}$ [25] is obtained from the approximated solution to Eqs. (4a) and (4b) in a slow light regime, where Δ_R changes slightly during the decay time on the order of $1/\gamma$. We take the photon detuning $\Delta_1 = 2\gamma$ and the pump detuning $\Delta_2 = -2\gamma$ under the EIT condition with $\Delta_R = 0$. The pulses' initial group velocity under the EIT condition is set as $v_g = 10 \text{ m/s}$ ($v_g = c/n_g$ with $n_g = n + \omega_p \partial n / \partial \omega_p$), while the pump Rabi frequency is $\Omega_c = 2\gamma$. The excited level $|e\rangle$ is $5P_{1/2}$ of ^{87}Rb . The dashed curve is that for the two-level system of the corresponding parameters. The minus signs of the horizontal axis labels come from our definition of Δ_1 . (b) Group velocity v_g vs Δ_R with the same pulse and pump detuning as in (a). The thicker solid curve is for $\Omega_c = 2\gamma$, whereas the thinner curve is about $\Omega_c = 4\gamma$. The dashed line is the group velocity of the corresponding two-level system.

The pulses will enter the superluminal regime characterized by anomalous dispersion [25], which is accompanied by huge dissipation, if the interaction-induced detuning Δ_R of the positive sign is gradually added to the pump beam of the system in Fig. 2. Equivalently, this phenomenon happens to the blue-detuned single-photon pulses in the presence of the attractive VdW potential. This danger of completely damping the input photons should be avoided in practice.

We, therefore, focus on red-detuned photons coupled to the ensemble and propagating toward each other under the attractive interaction. As the pulses get closer, they will expand spatially because the characteristic size of their distributions $\langle \hat{\Psi}_i^\dagger \hat{\Psi}_i \rangle(z, t)$ is proportional to the average of the distributed group velocity $v_g(z, t)$ over the pulses. This modifies the Δ_R value calculated with the relative distance and absorption of the pulses, which constantly keep changing as well. We use a numerical algorithm to simulate this dynamical process. From the coordinate origin $Z = 0$ situated on the center of one pulse, the longitudinal relative distance $-L \leq Z \leq L$ to the other pulse's center throughout their motion is divided into n_d grids. The detuning Δ_R at the i th ($0 < i \leq n_d - 1$) position is calculated with the pulse size and transmission rate at the $(i - 1)$ th position. Together with the obtained numerical values of Δ_R at the previous positions of $0 \leq k \leq i - 1$, it is plugged into Eq. (5) for the numerical integral to find the susceptibility $\chi^{(1)}$. In the same way, the updated group velocity and transmission rate from the susceptibility at the position i will be used to calculate the Δ_R value at the $(i + 1)$ th position. Running the iterative procedure with sufficiently large grid number n_d approaches the real pulse motion.

Figure 3 illustrates an example of pulse motion found by the above mentioned numerical method. As shown in Figs. 3(a) and 3(b), the greater interaction between more transversely adjacent pulses is inseparable with the more significant pulse losses. In the area where the Rydberg blockade starts to manifest, the accumulated pulse absorption has been harmful to the survival of the interacting photons [see Figs. 3(b) and 3(c)]. The pulse absorption rate and group velocity in the blockade regime tend to those for a two-level system with the corresponding system parameters, so the only way to reduce the pulse loss in the blockade regime is by the use of a higher photon detuning Δ_1 . However, one trade-off for doing so is to require a narrower pulse bandwidth (correspondingly a longer pulse size) to fit into the smaller EIT window, incurring a more prominent effect measured by the ratio $\delta_v(Z) = |\{v_g(Z, \sigma(Z)) - v_g(Z, 0)\} / v_g(Z, 0)|$ shown in Fig. 3(d). Here, $v_g(Z, \sigma(Z))$ is the group velocity at the location of the characteristic longitudinal size $\sigma(Z)$ from the pulse center, and $v_g(Z, 0)$ is that at the pulse center. The nonuniform group velocity distribution over pulses (in the comoving coordinate with the pulse centers) indicated by the ratio is equivalent to a group velocity dispersion that could make

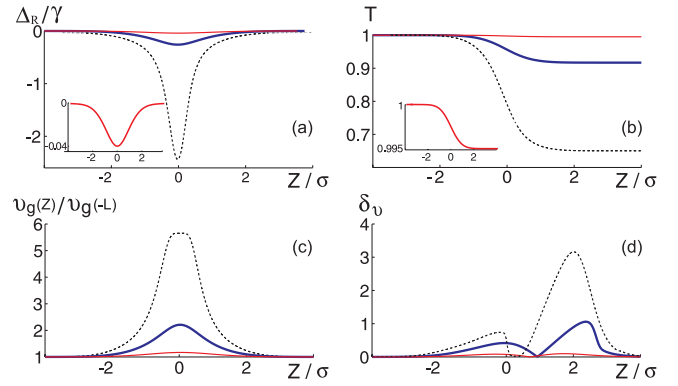


FIG. 3 (color online). Numerical simulation for pulse motion. Here, we adopt the relative distance coordinate Z as a substitute for the time scale. We use $|g\rangle = 5S_{1/2}$, $|e\rangle = 5P_{1/2}$, and $|r\rangle = 82D_{3/2}$ of ^{87}Rb , with the VdW coefficient $|C_6| = 8500 \text{ GHz } \mu\text{m}^6$ [26] and $\gamma = 2\pi \times 5.75 \text{ MHz}$. The system parameters are chosen as $Ng^2/\Omega_c^2 = 0.75 \times 10^7$ [$v_g(-L) = 10 \text{ m/s}$], $\Omega_c = 2\gamma$, and $\Delta_1 = -\Delta_2 = 2\gamma$. The input Gaussian shaped pulses with $f(z) = (1/\sqrt{\pi}\sigma)^{1/2} e^{-(1/2)z^2/\sigma^2}$ have the initial size $\sigma = 11.1 \mu\text{m}$, with the corresponding bandwidth well fitted into the EIT window. The dashed curves are about the transverse separation $a = 0.58\sigma$, the thicker solid ones for $a = \sigma$, and the thinner solid ones for $a = 1.5\sigma$. The iterative step size for the numerical simulation is 0.005σ . (a) Interaction-induced $\Delta_R(Z)$ at pulse centers. The insertion is the refined plot for $a = 1.5\sigma$. (b) Transmission rate $T(Z) = \exp(-k_p \int_{-L}^Z dy \text{Im}\{\chi^{(1)}(y)\})$. (c) Group velocity $v_g(Z) = c/n_g(Z)$ at pulse centers. The most transversely adjacent situation shows a velocity platform near the Rydberg blockade. (d) Group velocity deviation ratio $\delta_v(Z)$. For the same Z , more extending pulses have higher δ_v due to more spatially inhomogeneous interaction.

the pulses totally disappear even without absorption. Another disadvantage for large pulse size σ is that the detuning value Δ_R from the spatially distributed pulses (proportional to $1/\sigma^6$ for the VdW potential) will be below the magnitude for a significant XPM. Our results, thus, show that in the blockade regime considered in Ref. [20] the imperfections due to absorption and other factors are actually much more problematic.

The next target is to understand the real-time evolution of the DSP state $|1\rangle_1|1\rangle_2$ given before Eq. (1). Under the perfect EIT condition, there is the approximation $\langle \hat{\sigma}_{gr} \rangle = -\mu_{eg} E_l / \Omega_c$ ($\hat{\sigma}_{gr} = |g\rangle\langle r|$) or its quantum many-body version $\hat{S}_i(z) = -(g\sqrt{N}/\Omega_c)\hat{E}_i(z)$ after neglecting the nonadiabatic corrections for the narrow-band pulses, implying the identical propagation of the quantized DSP field with the electromagnetic field treated as classical in Eqs. (4a) and (4b) [25]. In the suitable weak interaction regime, we find for the two-photon process, such as the most transversely separated pulses in Fig. 3 [corresponding to the refractive curves close to that of $\Delta_R = 0$ in Fig. 2(a)], this approximation still holds with a small ratio Δ_R/Ω_c . The kinetic Hamiltonian for the slowly moving DSPs in the weak interaction regime can, therefore, be constructed as

$H_K = -\sum_l i v_{g,l}(t) \int dz \hat{\Psi}_l^\dagger(z) \partial_z \hat{\Psi}_l(z)$, where the group velocity $v_{g,l}(t)$ is determined with Eqs. (4a) and (4b). Meanwhile, for slow light with $\cos \theta \ll 1$, the BSPs interact very slightly with the DSPs and among themselves because they contain negligible Rydberg excitation. Their quick decoupling from the system and decaying into the environment allow one to treat the BSPs as motionless oscillations, though their group velocities can be read from their spectrum in Eq. (1).

Our method for pulse state evolution is to adopt the joint evolution $U(t, 0)$ as the time-ordered exponential $T e^{-i \int_0^t d\tau \{H(\tau) + H_D(\tau)\}}$ on the initial state $|\psi_{\text{in}}\rangle = |1\rangle_1 |1\rangle_2 |0\rangle_c$ as the product of the input pulse state and the reservoir vacuum state $|0\rangle_c$. Tracing out the reservoir degrees of freedom in the evolved state $U(t, 0)|\psi_{\text{in}}\rangle$ gives the evolved system state. We have three noncommutative items (H_K , H_{AF} , and H_I) in $H(t)$ as well as the dissipation Hamiltonian $H_D(t)$ of Eq. (3), for the joint evolution operator $U(t, 0)$. Directly applying $U(t, 0)$ on the DSP operators in $|\psi_{\text{in}}\rangle$ is impossible, as it is equivalent to analytically solving a nonlinear Langevin equation. One technique to circumvent the difficulty is the factorization of an evolution operator into the relatively tractable ones [27]. For our problem, we have $U(t, 0) = U_K(t, 0)U_{\text{AF}}(t, 0)U_I(t, 0)U_D(t, 0)$ (see the Supplemental Material [28]). Among the factorized processes $U_X(t, 0) = T \exp\{-i \int_0^t d\tau \tilde{H}_X(\tau)\}$, for $X = K, \text{AF}, I$, and D , \tilde{H}_K and \tilde{H}_D are indifferent to their original form H_K and H_D , respectively. The operator $U_D(t, 0)$ takes no effect on $|\psi_{\text{in}}\rangle$, but the noncommutativity of H_D with H_{AF} makes the BSP field operators in H_{AF} become those in \tilde{H}_{AF} as follows:

$$\hat{\Phi}_{\pm,l}(z) \rightarrow \hat{\Xi}_{\pm,l}(z, \tau) = e^{-\phi_{\pm}^2 \gamma (t-\tau)/2} \hat{\Phi}_{\pm,l}(z) \pm \sqrt{\gamma} \phi_{\pm} \int_{\tau}^t dt' e^{-\phi_{\pm}^2 \gamma (t'-\tau)/2} \hat{\xi}_l(z), \quad (6)$$

where $\phi_{+(-)} = \cos \phi (\sin \phi)$. A sufficiently large γ value approximates the commutator $[\hat{\Xi}_{\pm,l}(z, \tau_1), \hat{\Xi}_{\pm,l}(z', \tau_2)] = e^{-\gamma \phi_{\pm} |\tau_1 - \tau_2|} \delta(z - z')$ as vanishing for $\tau_1 \neq \tau_2$. Under this approximation, the BSP operators in $U_I(t, 0)$ also take the forms in Eq. (6), hence, the evolved state $\hat{U}_I(t, 0)|\psi_{\text{in}}\rangle$,

$$\left\{ \int dz_1 dz_2 f(z_1) f(z_2) e^{-ic_3^4 \int_0^t d\tau \Delta(z_1^\dagger - z_2^\dagger)} \hat{\Psi}_1^\dagger(z_1) \hat{\Psi}_2^\dagger(z_2) - ic_3^3 \sum_{l=1}^2 \int_0^t d\tau \int dz_1 dz_2 f(z_1) f(z_2) e^{-ic_3^4 \int_0^t d\tau \Delta(z_1^\dagger - z_2^\dagger)} \times \Delta(z_1^\dagger - z_2^\dagger) (c_1 \hat{\Xi}_{+,l}^\dagger + c_2 \hat{\Xi}_{-,l}^\dagger)(z_1, \tau) \hat{\Psi}_{3-l}^\dagger(z_2) \right\} |0\rangle_l, \quad (7)$$

(un-normalized) to the first order of $\cos \theta$, where the notations $c_1 = \cos \theta \sin \phi$, $c_2 = \cos \theta \cos \phi$, $c_3 = \sin \theta$,

$z^\tau = z + \int_0^\tau dt' v_{g,l}(t')$, and $|0\rangle_l = |0\rangle|0\rangle_c$ are used to simplify the result. The detailed procedure for deriving the evolved state is given in the Supplemental Material [28]. The succeeding operation U_{AF} only affects the BSP components in Eq. (7), whereas U_K displaces the coordinate of $\hat{\Psi}_l^\dagger(z_l)$.

The interaction potential $\Delta(z_1 - z_2)$ renders the DSP part in Eq. (7) no longer factorizable with respect to z_1 and z_2 . This entangled piece deviates from the ideal output state $e^{i\varphi} |1\rangle_1 |1\rangle_2$ with a uniform phase φ . We measure the degrees of such deviation by comparing the real output $|\psi_{\text{out}}\rangle = U(t, 0)|\psi_{\text{in}}\rangle$ with a reference state $|\psi_{\text{out}}^0\rangle = U_K(t, 0)U_{\text{AF}}(t, 0)U_D(t, 0)|\psi_{\text{in}}\rangle$. In the absence of $U_I(t, 0)$, this reference remains in the product state $|1\rangle_1 |1\rangle_2 |0\rangle_c$, even if the amplitude $f_l(z_l)$ in the output photon state $|1\rangle_l$ is lowered due to any residual absorption. The output's fidelity F with the ideal one and the associate cross phase φ can, thus, be found from the overlap $\sqrt{F} e^{i\varphi} = \langle \psi_{\text{out}}^0 | \psi_{\text{out}} \rangle$, where the two output states are normalized. Similar definitions for F and φ can be found in Refs. [29,30].

In Fig. 4, we plot the fidelity and cross phase for the most transversely separated pulses in Fig. 3. Because of the steep decay of the VdW potential at long distances, both fidelity and cross phase for the counterpropagation in Fig. 4(a) quickly converge to fixed values with increasing medium size. A cross phase of π rad that still keeps close to unit F can be achieved if the VdW coefficient $|C_6|$, for example, is lifted by about 9 times with a different Rydberg level. Contrary to a widely held notion, counterpropagation does not automatically ensure high fidelity; see Ref. [30]. The inset of Fig. 4(a) shows the fidelity for an imagined motion of two pulses passing each other very slowly. The same propagation geometry indicates that the degrading fidelity in the slow motion comes from the growing pulse entanglement over a longer interaction time. In comparison, we also study the copropagating pulses in Fig. 4(b). The copropagation exhibits considerable trade-off between F

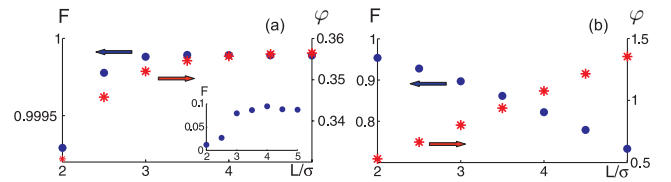


FIG. 4 (color online). (a) Fidelity and cross phase of photon-photon XPM for two counterpropagating pulses with the transverse separation $a = 1.5\sigma$ in Fig. 3. L is the medium size. The system parameters are the same as in Fig. 3. The inset describes an imagined situation by reducing the initial pulse velocity to 10^{-2} m/s. (b) Fidelity and cross phase for two pulses propagating together along two tracks separated by $a = 1.5\sigma$. Because of pulse absorption, their group velocity is not stable in such copropagation (for example, it drops from 11.007 to 11.002 m/s from $L = 2\sigma$ to 5σ).

and φ and would be unfavorable for making large phases of good quality.

In summary, we have studied the process of two-photon interaction via a Rydberg atomic ensemble. Our approach based on the complete dynamics for both single atoms and ensemble enables a more realistic description of the situation without steady state. The previously considered regime near the Rydberg blockade is found to be short of the favorable figures of merit for photon-photon XPM. We also prove that approximately ideal XPM creating a considerable nonlinear phase can be realized with counterpropagating and transversely separated pulses that weakly interact with each other. The photon-photon XPM we have discussed can be the basis for an all-optical deterministic quantum phase gate.

B. H. and C. S. acknowledge the support by AITF and NSERC. M. X. acknowledges the support in part by NBRPC (Grant No. 2012CB921804) and NSFC (Grant No. 11321063). A. V. S. was supported by RFBR 12-02-31621.

*mxiao@uark.edu

- [1] H. Schempp, G. Günter, C. S. Hofmann, C. Giese, S. D. Saliba, B. D. DePaola, T. Amthor, M. Weidemüller, S. Sevinçli, and T. Pohl, *Phys. Rev. Lett.* **104**, 173602 (2010).
- [2] J. D. Pritchard, D. Maxwell, A. Gauguier, K. J. Weatherill, M. P. A. Jones, and C. S. Adams, *Phys. Rev. Lett.* **105**, 193603 (2010).
- [3] T. Peyronel, O. Firstenberg, Q.-Y. Liang, S. Hofferberth, A. V. Gorshkov, T. Pohl, M. D. Lukin, and V. Vuletić, *Nature (London)* **488**, 57 (2012).
- [4] Y. O. Dudin and A. Kuzmich, *Science* **336**, 887 (2012).
- [5] D. Maxwell, D. Szwer, D. Paredes-Barato, H. Busche, J. Pritchard, A. Gauguier, K. Weatherill, M. Jones, and C. Adams, *Phys. Rev. Lett.* **110**, 103001 (2013).
- [6] C. S. Hofmann, G. Günter, H. Schempp, M. Robert-de-Saint-Vincent, M. Gärtner, J. Evers, S. Whitlock, and M. Weidemüller, *Phys. Rev. Lett.* **110**, 203601 (2013).
- [7] O. Firstenberg, T. Peyronel, Q.-Y. Liang, A. V. Gorshkov, M. D. Lukin, and V. Vuletić, *Nature (London)* **502**, 71 (2013).
- [8] C. Ates, S. Sevinçli, and T. Pohl, *Phys. Rev. A* **83**, 041802 (R) (2011).
- [9] S. Sevinçli, N. Henkel, C. Ates, and T. Pohl, *Phys. Rev. Lett.* **107**, 153001 (2011).
- [10] D. Petrosyan, J. Otterbach, and M. Fleischhauer, *Phys. Rev. Lett.* **107**, 213601 (2011).
- [11] J. D. Pritchard, C. S. Adams, and K. Mølmer, *Phys. Rev. Lett.* **108**, 043601 (2012).
- [12] D. Yan, Y.-M. Liu, Q.-Q. Bao, C.-B. Fu, and J.-H. Wu, *Phys. Rev. A* **86**, 023828 (2012).
- [13] D. Petrosyan and K. Mølmer, *Phys. Rev. A* **87**, 033416 (2013).
- [14] M. Gärtner and J. Evers, *Phys. Rev. A* **88**, 033417 (2013).
- [15] A. V. Gorshkov, R. Nath, and T. Pohl, *Phys. Rev. Lett.* **110**, 153601 (2013).
- [16] J. Otterbach, M. Moos, D. Muth, and M. Fleischhauer, *Phys. Rev. Lett.* **111**, 113001 (2013).
- [17] J. Stanojevic, V. Parigi, E. Bimbard, A. Ourjoumtsev, and P. Grangier, *Phys. Rev. A* **88**, 053845 (2013).
- [18] I. Friedler, D. Petrosyan, M. Fleischhauer, and G. Kurizki, *Phys. Rev. A* **72**, 043803 (2005).
- [19] B. He, A. MacRae, Y. Han, A. I. Lvovsky, and C. Simon, *Phys. Rev. A* **83**, 022312 (2011).
- [20] A. V. Gorshkov, J. Otterbach, M. Fleischhauer, T. Pohl, and M. D. Lukin, *Phys. Rev. Lett.* **107**, 133602 (2011).
- [21] E. Shahmoon, G. Kurizki, M. Fleischhauer, and D. Petrosyan, *Phys. Rev. A* **83**, 033806 (2011).
- [22] M. Fleischhauer and M. D. Lukin, *Phys. Rev. Lett.* **84**, 5094 (2000).
- [23] C. W. Gardiner and P. Zoller, *Quantum Noise* (Springer-Verlag, Berlin, 2000).
- [24] J. Gea-Banacloche, Y. Q. Li, S. Z. Jin, and M. Xiao, *Phys. Rev. A* **51**, 576 (1995); M. Xiao, Y. Q. Li, S. Z. Jin, and J. Gea-Banacloche, *Phys. Rev. Lett.* **74**, 666 (1995).
- [25] P. W. Milloni, *Fast Light, Slow Light and Left-Handed Light* (IOP Publishing Ltd., Bristol and Philadelphia, 2005).
- [26] L. Béguin, A. Vernier, R. Chicireanu, T. Lahaye, and A. Browaeys, *Phys. Rev. Lett.* **110**, 263201 (2013).
- [27] B. He, *Phys. Rev. A* **85**, 063820 (2012).
- [28] See the Supplemental Material at <http://link.aps.org/supplemental/10.1103/PhysRevLett.112.133606> for details.
- [29] J. Gea-Banacloche, *Phys. Rev. A* **81**, 043823 (2010).
- [30] B. He and A. Scherer, *Phys. Rev. A* **85**, 033814 (2012).